Local Magnetic Moment Associated with an Iron Atom Dissolved in Various Transition Metal Alloys

A. M. CLOGSTON, B. T. MATTHIAS, M. PETER, H. J. WILLIAMS, E. CORENZWIT, AND R. C. SHERWOOD
Bell Telephone Laboratories, Inc., Murray Hill, New Jersey

(Received August 29, 1961)

One atomic percent of iron has been dissolved in a series of alloys of the second row transition metals. The alloys have been chosen so as to give closely spaced coverage from zirconium to beyond palladium. For each dilute iron alloy, the susceptibility χ has been measured from 1.4°K to room temperature. In some members of the series, the susceptibility is essentially temperature independent, while in others the appearance of a local moment is evidenced by a Curie-Weiss dependence of χ on T. A local moment first appears proceeding from Nb to Mo at about $(Nb_{0.6}Mo_{0.4})_{0.99}Fe_{0.01}$ and persists nearly to Re. Disappearing at this point, the moment reappears at $(Ru_{0.75}Rh_{0.25})_{0.99}Fe_{0.01}$ and continues, becoming large in the alloys near Pd. The occurrence of local moments is discussed in terms of the band structure of the alloys and the perturbation introduced by the iron atom. The giant magnetic moments observed near Pd are related to the large susceptibilities of the iron-free alloys in this region.

I. INTRODUCTION

IN a previous paper[1] we have described observations made of the susceptibility and superconducting transition temperature of a series of second row transition metal alloys containing a small amount of iron. The alloys were composed of various proportions of niobium and molybdenum with the addition of one atomic percent of iron in each case. It was reported that the alloys close to niobium in composition showed an essentially temperature-independent susceptibility, nearly equal to that of the Nb—Mo matrix, over the range from 1.4°K to room temperature. In marked contrast, it was also observed that the alloys near molybdenum in composition showed a strongly temperature-dependent susceptibility not seen in the absence of iron. It was possible to fit this suceptibility in a satisfactory manner to a Curie-Weiss law of the form

$$\chi=\frac{np^2\mu_B^2}{3k(T-\theta)}, \qquad (1)$$

where n is the number of magnetic centers, p is the effective magnetic moment given by $g[S(S+1)]^{\frac{1}{2}}$, and θ is the Curie temperature. In reference 1, this Curie-Weiss behavior was interpreted to mean that, in molybdenum, each iron atom possessed a local magnetic moment, whereas this moment failed to appear when iron was dissolved in niobium. In Fig. 2 of reference 1 a curve was given showing how the local moment appeared as the concentration of molybdenum increased. The most striking feature of the curve was that the moment appeared abruptly at about 40 at. % molybdenum and rose steeply but continuously to its maximum value.

A localized moment was also observed somewhat beyond molybdenum in the alloy $(Mo_{0.8}Re_{0.2})_{0.99}Fe_{0.01}$. In the absence of iron, this alloy is a good superconductor,[2] but the presence of very small amounts of iron sharply reduces the transition temperature. This is consistent with the presence of a local magnetic moment.[3,4] In contrast, in the case of niobium where no local moment was observed, a corresponding amount of iron was found to have negligible effect upon the superconducting transition temperature.

In this paper we present experiments that extend the work of Reference 1 to nearly the whole extent of the second transition period from zirconium to beyond palladium. In most cases, however, it has been necessary to use rhenium instead of technetium. We now report that the local moment appearing between niobium and molybdenum disappears at rhenium, reappears just beyond ruthenium, becomes very large at palladium in agreement with previous work,[5–7] and then becomes smaller again moving towards silver.

The quantum mechanical nature of a localized magnetic moment in a metal has been considerably clarified in papers by Anderson[8] and Wolff[9] since the appearance of our earlier results. We shall make use of some of these results in giving an interpretation of our experiments in terms of the band structure of the transition metals and the perturbation introduced into the lattice by the iron nucleus. We shall also offer an explanation of the giant magnetic moments observed by us and others in the alloys near palladium.

II. MEASUREMENTS AND MATERIALS

In these experiments, the susceptibility of the various alloys was measured at a field of 14 000 gauss over the temperature range 1.4°K to room temperature in an apparatus previously described.[10]

[1] B. T. Matthias, M. Peter, H. J. Williams, A. M. Clogston, E. Corenzwit, and R. C. Sherwood, Phys. Rev. Letters **5**, 542 (1960).
[2] J. K. Hulm, Phys. Rev. **98**, 1539 (1955).
[3] B. T. Matthias, H. Suhl, and E. Corenzwit, Phys. Rev. Letters **1**, 92 (1958).
[4] H. Suhl and B. T. Matthias, Phys. Rev. **114**, 977 (1959).
[5] D. Gerstenberg, Ann. Physik **2**, 236 (1958).
[6] J. Crangle, Phil. Mag. **5**, 335 (1960).
[7] R. M. Bozorth, P. A. Wolff, D. D. Davis, V. B. Compton, and J. H. Wernick, Phys. Rev. **122**, 1157 (1961).
[8] P. W. Anderson, Phys. Rev. **124**, 41 (1961)
[9] P. A. Wolff, Phys. Rev. **124**, 1030 (1961).
[10] R. M. Bozorth, H. J. Williams, and D. E. Walsh, Phys. Rev. **103**, 572 (1956).

The samples were prepared by fusion of the elements in an argon arc furnace. The furnace was suspended so that it could be continually agitated while the samples were in the molten state. The ingots were remelted most usually between six and eight times.

The weight loss of the melts never exceeded $\frac{1}{2}\%$ which was unimportant except in those alloys which contained small amounts of iron. In this case, special care was taken not to exceed the melting point of the matrix more than necessary. In these alloys the total weight loss was never more than 10% of the added iron, and errors of this order may be present in the indicated concentrations based on starting materials. No wet analyses were made to obtain exact compositions, but x-ray fluorescence analyses confirmed the nominal compositions. All melts containing iron were annealed at 1200°C for one week.

The molybdenum and rhenium used in the experiments was in the form of rods of purity 99.99%. The palladium was in the form of sponge of purity 99.999%, while the purity of the rhodium and ruthenium sponge was 99.9%. The iron was electrolytic of purity better than 99.999%. Zirconium was obtained in the form of crystalline bars. While its oxygen content was not known, purity was better than 99.9%. A similar grade of purity was available for scandium and niobium. Vanadium was obtained as a large conglomerate of crystals and was certainly of purity not better than 98.5%. The impurities, however, are almost entirely N_2 and O_2 and are largely lost during melting of the alloys. No impurities were introduced by the arc melting since x-ray fluorescence did not detect any traces of W (the cathode) or of Cu (the anode).

III. EXPERIMENTAL RESULTS

The principal results of our experiments involving the alloying of adjacent members of the second long transition period are presented in Tables I and II and in Fig. 1. In the two tables we have listed the various alloys studied, along with the average number of electrons N per atom outside the closed $4p$ shell. Each alloy is to be understood as containing one atomic percent of iron. In Table I, covering the alloys from Zr to Ru, the first four and last four entries had essentially temperature independent susceptibilities. In the remaining cases the susceptibility χ increased markedly at low temperatures. We have fitted χ to a Curie-Weiss law as given in Eq. (1) as follows. In this region of the periodic table the susceptibility of the various alloys in the absence of iron, χ_0, is nearly temperature independent. We have determined χ_0 in each case by plotting χ vs $1/T$ and extrapolating to $T=\infty$. We then plot $1/(\chi-\chi_0)$ as a function of temperature and determine p from the slope and θ from the intersection with the temperature axis. As an example we show in Fig. 2, $1/(\chi-\chi_0)$ plotted against T for the alloy $Mo_{0.99}Fe_{0.01}$. In Table I we have listed for each alloy θ and the quantity $\mu/\mu_B=gS$ which is obtained from p by assuming that $g=2$. We estimate the accuracy of μ/μ_B to be about $\pm 5\%$. The values of θ are estimated to be

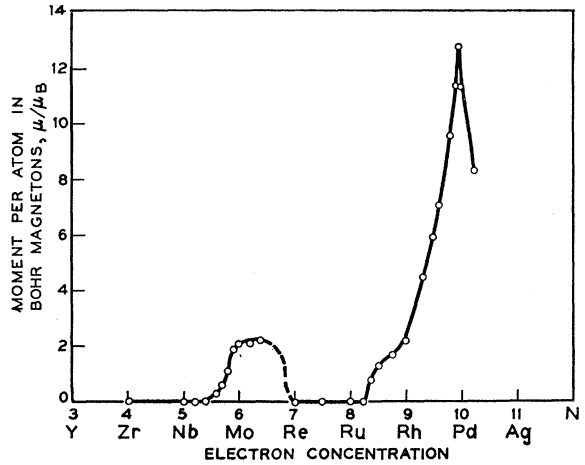

FIG. 1. Magnetic moment in Bohr magnetons of an iron atom dissolved in various second row transition metals and alloys as a function of electron concentration.

TABLE I. Magnetic moment and Curie temperature for 1% solutions of Fe in $4d$ alloys from Zr to Ru.

Alloy	Structure	N	μ/μ_B (Curie-Weiss)	θ (°K)
Zr	hcp	4	0.0	
Nb	bcc	5	0.0	
$Nb_{0.8}Mo_{0.2}$	bcc	5.2	0.0	
$Nb_{0.6}Mo_{0.4}$	bcc	5.4	0.0	
$Nb_{0.4}Mo_{0.6}$	bcc	5.6	0.3	-9 ± 3
$Nb_{0.3}Mo_{0.7}$	bcc	5.7	0.6	-4
$Nb_{0.2}Mo_{0.8}$	bcc	5.8	1.1	-1
$Nb_{0.1}Mo_{0.9}$	bcc	5.9	1.9	-3
Mo	bcc	6.0	2.1	-4
$Mo_{0.8}Re_{0.2}$	bcc	6.2	2.1	-6
$Mo_{0.6}Re_{0.4}$	bcc	6.4	2.2	-5
Re	hcp	7.0	0.0	
Tc	hcp	7.0	0.0	
$Re_{0.5}Ru_{0.5}$	hcp	7.5	0.0	
Ru	hcp	8.0	0.0	

TABLE II. Magnetic moment and Curie temperature for 1% solutions of Fe in $4d$ alloys from Ru to Pd.

Alloy	Structure	N	μ/μ_B (Curie-Weiss)	θ (°K)	μ/μ_B (Sat. mag.)	T_c (°K)
Ru	hcp	8.0	0.0			
$Ru_{0.75}Rh_{0.25}$	hcp	8.25	0.0			
$Ru_{0.63}Rh_{0.37}$	hcp	8.37	0.8	-21 ± 2		
$Ru_{0.5}Rh_{0.5}$	hcp	8.5	1.3	-13 ± 2		
$Ru_{0.25}Rh_{0.75}$	fcc	8.75	1.7	-17 ± 2		
Rh	fcc	9.0	2.2	-14 ± 2		
$Rh_{0.7}Pd_{0.3}$	fcc	9.3	4.5	-2		
$Rh_{0.55}Pd_{0.45}$	fcc	9.45	5.9(100°K)	-2		
$Rh_{0.4}Pd_{0.6}$	fcc	9.6	7.1(100°K)	1		
$Rh_{0.2}Pd_{0.8}$	fcc	9.8	9.6(100°K)	14	7.1	11
$Rh_{0.1}Pd_{0.9}$	fcc	9.9	11.4(100°K)	33 ± 2	9.5	27
$Rh_{0.05}Pd_{0.95}$	fcc	9.95	12.7(100°K)	49 ± 6	10.8	39
Pd	fcc	10.0	11.3(100°K)	55 ± 3	9.7	39
$Pd_{0.75}Ag_{0.25}$	fcc	10.25	8.3(100°K)	12	6.3	11

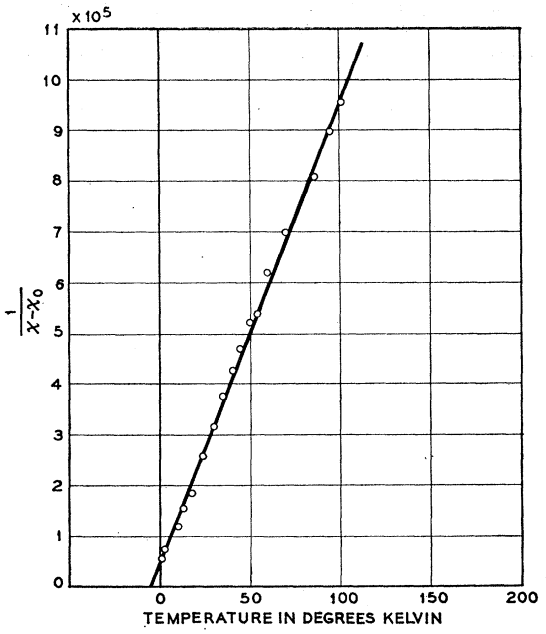

FIG. 2. Reciprocal susceptibility of the alloy $Mo_{0.99}Fe_{0.01}$ plotted as a function of absolute temperature.

accurate to about ±1°K except in those cases where a larger error is indicated.

It was unfortunately not possible to prepare alloys of Mo and Re beyond $Mo_{0.6}Re_{0.4}$ because of the appearance of a new crystalline phase. This portion of Fig. 1 has, however, been covered by a different system as will be noted below.

Although some technetium was available during the course of these experiments, the difficulty of working with this material precluded making an extensive series of alloys to compare with the behavior of the Re alloys. We report just one case, $Tc_{0.99}Fe_{0.01}$, in which no local moment was observed, similarly to the Re case. The superconducting transition temperature was lower than that for Tc by about 0.5°C.

In Table II we present results obtained for the alloys from Ru to $Pd_{0.75}Ag_{0.25}$. For these systems, the susceptibility of the matrix was sufficiently temperature dependent so that a separate measurement was made of χ_0 in each case as a function of T. The corrected susceptibility $(\chi-\chi_0)$ was then used as before to determine μ/μ_B and θ. This procedure gave reasonable results up to $Rh_{0.7}Pd_{0.3}$, yielding the values of μ/μ_B and θ given in Table II. It is of interest to compare the values of μ/μ_B with those given in Table I. As can be seen in Fig. 1, the initial rise of μ/μ_B at $N=8.25$ is comparable to the rise at $N=5.5$, and even gives an impression of leveling out near 2 Bohr magnetons. Beyond rhodium, however, μ/μ_B begins increasing to large values. These large moments are related to the large saturation moments per atom of solute reported by Gerstenberg[5] for Mn, Fe, Co and Ni in Pd, by Crangle[6] for Fe in Pd, and by Bozorth *et al.*[7] for Co in Pd. It appears evident that the spin of the iron impurity is polarizing the matrix in its vicinity to give an enhanced local moment. A theoretical discussion of these giant moments will be given below.

Beyond $Rh_{0.7}Pd_{0.3}$, we encounter a new situation. First of all, the susceptibility of the matrix becomes a strong function of the temperature as can be seen in Fig. 3, which shows measurements of χ_0 taken on alloys of Rh—Pd by Budworth, Hoare, and Preston.[11] It becomes empirically evident that the simple correction introduced above is no longer adequate. As an example, we show in Fig. 4 the result of plotting $1/(\chi-\chi_0)$ against T for $Rh_{0.1}Pd_{0.9}$. The shape of the curve as it stands precludes a meaningful fit to a Curie-Weiss law. We have proceeded, therefore, phenomenologically as follows. We suppose that the local magnetic moment associated with each iron atom is proportional to the susceptibility χ_0 of the matrix. If these moments are large, as is true in the present alloys, we may write approximately

$$p=p_r(\chi_0/\chi_{0r}), \tag{2}$$

where p_r designates the moment and susceptibility at some reference temperature T_r. We may then rewrite Eq. (1) as

$$\frac{(\chi_0/\chi_{0r})^2}{\chi-\chi_0}=\frac{3k(T-\theta)}{np_r^2\mu_B^2}. \tag{3}$$

In Fig. 4 we have also plotted the left hand side of Equation (3) as a function of T, using 100°K as the reference temperature. The resulting curve is satisfactorily straight and permits the determination of θ and

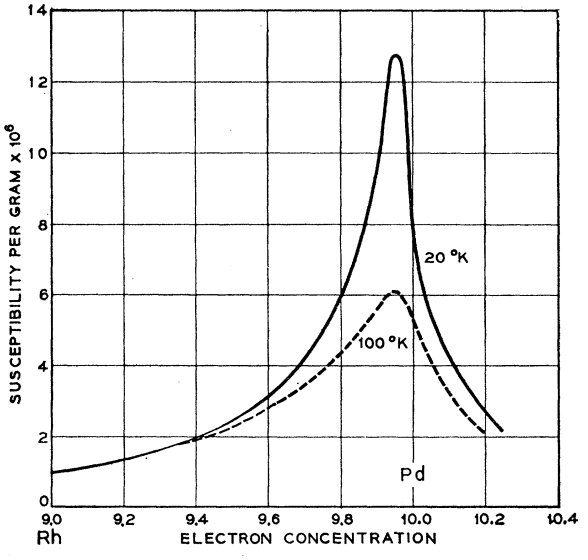

FIG. 3. Susceptibility per gram for various rhodium-palladium alloys at 20°K and 100°K according to Budworth, Hoare, and Preston.

[11] D. W. Budworth, F. E. Hoare, and J. Preston, Proc. Roy. Soc. A257, 250 (1961).

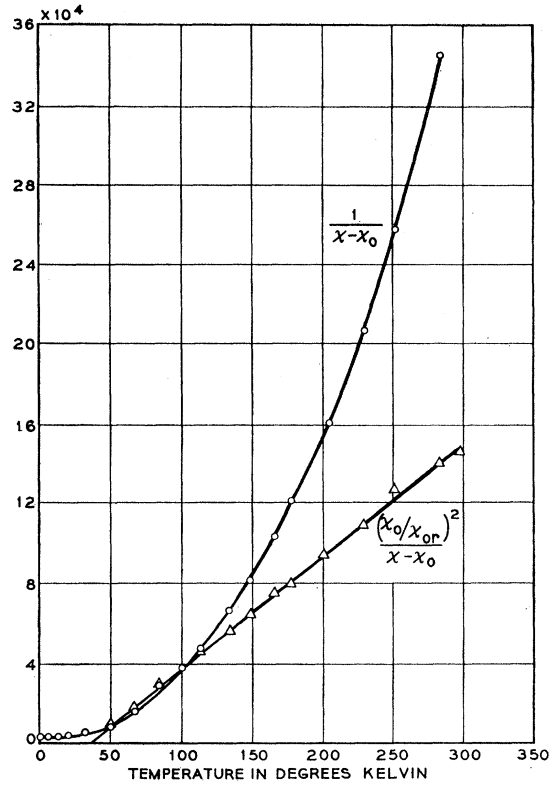

FIG. 4. Reciprocal susceptibility $1/(\chi-\chi_0)$ for the alloy $(Rh_{0.7}Pd_{0.3})_{0.99}Fe_{0.01}$. Also shown is the reciprocal susceptibility modified as described in the text.

p(100°K). In this way we have determined μ(100°K) and θ for the alloys beyond $Rh_{0.6}Pd_{0.4}$ and obtained the values listed in Table II and presented in Fig. 1. Not all the curves of $(\chi/\chi_{0r})^2/(\chi-\chi_0)$ were as straight as the one shown in Fig. 4, but were close enough to a straight line to permit the determination of p(100°K) to an accuracy better than ±5%. The measurements of χ_0 used in making these reductions were obtained on specimens prepared in identical fashion to the dilute iron alloys, and were in fair agreement with the measurements of Budworth, Hoare, and Preston.[11]

A curve similar to Fig. 4 has been given by Gerstenberg[5] for $Pd_{0.99}Fe_{0.01}$ for temperatures extending up to 1100°K. Above 400°K this curve is approximately a straight line and has been used by Gerstenberg to determine a Curie temperature of 238°K and a p value equal to 4.94 μ_B. It is evident from the discussion above that this proceedure has little meaning. In particular, the Curie temperature determined in this way can only be considered an artifact, and this is confirmed by the high value obtained by Gerstenberg.

As long as Eq. (2) can be considered valid, p will be a function of temperature and can be obtained for any temperature from p_r by appropriate use of Eq. (2). It can also be obtained from the plot of $1/(\chi-\chi_0)$ vs T. The slope of the straight line passing through the temperature axis at $T=\theta$ and intersecting the curve at the particular temperature in question determines $p(T)$. This provides a graphical picture of how p decreases with increasing temperature, and shows that the slope used by Gerstenberg does not give a correct moment at any temperature. It will be noted in Fig. 4 that the points near 80°K lie above the curves. The anomaly is not accidental and was observed in the four alloys beyond and including $Rh_{0.2}Pd_{0.8}$. This temperature seems to correspond to the susceptibility maximum observed in Pd near 80°K.[11]

TABLE III. Magnetic moment and Curie temperature for 1% solutions of Fe in various alloys.

Alloy	Structure	N	μ/μ_B (Curie-Weiss)	θ (°K)
$V_{0.67}Ru_{0.33}$	CsCl	6.0	1.1	−3
$V_{0.6}Ru_{0.4}$		6.2	2.4	−4
$V_{0.5}Ru_{0.5}$	tetra.	6.5	2.2	−2
$Mo_{0.75}Rh_{0.25}$	hcp	6.75	1.9	−27±2
$Mo_{0.72}Rh_{0.28}$	hcp	6.84	0.7	−4
$Mo_{0.9}Pd_{0.1}$	bcc	6.4	11.2	−33
$Mo_{0.8}Pd_{0.2}$	bcc	6.8	6.0	−10
$Mo_{0.6}Pd_{0.4}$	bcc	7.6	2.6	−5
$Mo_{0.45}Pd_{0.55}$	bbc+fcc	8.2	3.0	−15
$Mo_{0.4}Pd_{0.6}$	fcc	8.4	4.1	−9
$Mo_{0.2}Pd_{0.8}$	fcc	9.2	6.1	0

The alloys beyond $Rh_{0.6}Pd_{0.4}$ are ferromagnetic at low temperatures and we have included in Table II the observed saturation moment per atom of iron and the Curie temperature T_c obtained by the method of plotting H/σ_g vs σ_g^2, where σ_g is the magnetization per gram. The results for Pd are in reasonable agreement with the measurements of Crangle[6] whose lowest iron concentration was 1.25 at. %. For this alloy he found a saturation magnetization of 7.4 Bohr magnetons per atom of iron and a Curie temperature of 66°K. The results given in Table II for θ and T_c, and for μ/μ_B determined in the ferromagnetic and paramagnetic regions, are in qualitative agreement and give support to our method of analyzing the paramagnetic susceptibility.

In addition to the main sequence of alloys presented in Tables I and II, we have investigated the behavior of various other systems, partly to fill in various gaps in the picture, and partly to test to what extent alloys with the same electron concentration but different composition will correspond to Fig. 1. These results are collected in Table III and shown superimposed on the curve of Fig. 1 in Fig. 5.

It will be observed that the vanadium-ruthenium alloys and molybdenum-rhodium alloys taken together trace out a curve similar in shape to the peak defined by the Nb-Mo-Re alloys of Fig. 1. It has already been reported that iron dissolved in vanadium shows no localized moment.[1] The corresponding behavior of these different systems when plotted as a function of electron concentration suggests that the band structures of all these alloys are similar and that the rigid band model is a fair approximation. It is very interesting to note that neither V or Ru separately show a local

moment for dissolved iron, but that the V-Ru alloys do show such a moment over a considerable range of composition.

The data for the Mo-Pd dilute iron alloys are particularly striking. Although the observed moments do not fit on the curve of Fig. 1, there is a deep minimum that corresponds well with the region where no local moment exists in the Re-Ru dilute iron system. Outside this region the local moment becomes very large both towards Mo and Pd. The experiment seems to indicate that giant local moments are associated with the presence of Pd whatever the average electron concentration of the alloy. Mo and Pd are so far apart in the periodic table that the rigid band model can have little meaning for their alloys and the discussion of these systems will be very complicated.

Finally, we have made some preliminary investigations of the alloys near $N=3$. We were not successful in forming solid solutions of iron in yttrium. We have, however, investigated a solution of 1 at. % iron in Sc. The addition of iron greatly increases the susceptibility at low temperatures and suggests that a large local moment exists in this alloy. We have not as yet been able to interpret these curves in such a way as to assign an unambiguous value to the moment.

IV. INTERPRETATION

The results that are reported in this paper show clearly that, in some portions of the periodic table, an iron nucleus present as a dilute impurity in a host lattice has associated with it a localized magnetic moment. This experimental fact has two implications: first, there must be wave functions associated with the iron atoms that are local in character, as distinguished from band wave functions having equal amplitude in each unit cell throughout the body of the crystal; and secondly, these local wave functions have a net spin and show a magnetic moment of several Bohr magnetons. In this section, we would like to discuss first the nature of local states in metals, next the circumstances under which the local states will magnetize, and then the application of these ideas to the occurrence of local moments in the 4*d* transition metals. Finally, we shall consider the origin of the giant moments observed in the alloys near palladium.

A. Localization of States

The nature of localized states around impurities in metals and semiconductors has been the subject of much discussion. The problem is rather different in the two cases because the high density of conduction electrons in a metal usually causes the local state to be very closely confined about the impurity center. In contrast, in a semiconductor the impurity state may spread out over many lattice sites. An extensive discussion has been given of the metallic case by Friedel[12] using a model based upon a free-electron conduction band. His main argument proceeds as follows. An electron is incident upon the impurity center characterized by a nuclear charge Z units larger than the nuclear charge of the host atoms, and is scattered. The outgoing wave is analyzed into angular momentum components of quantum number l, each of which shows a phase shift γ_l compared to its phase in the absence of the impurity. The density of states in energy is shown to be shifted by an amount $(1/\pi)d\gamma_l/dE$ for each component by considering boundary conditions on the waves at the surface of a very large sphere surrounding the impurity. Consequently, the total number of new states below energy E, considering degeneracies, is $(1/\pi)\sum_l (2l+1)\times\gamma_l(E)$. Since two electrons of opposite spin may occupy each state, and since the crystal must remain electrically neutral one can write

$$Z=-\frac{2}{\pi}\sum_l (2l+1)\gamma_l(E_f), \tag{4}$$

where E_f is the Fermi energy. This is Friedel's phase rule. In many cases the shielding charge is not uniformly distributed in energy. Thus, if there is an energy where $d\gamma_l/dE$ is large, there will be an accumulation of states in a narrow energy range. Such a region is called a virtual state and has a width determined by $d\gamma_l/dE$. The wave functions contributing to such a virtual state are concentrated about the impurity and constitute what we mean by a local state. In some cases, the energy at which $d\gamma_l/dE$ is large may lie below the edge of the band, in which instance the state is infinitely narrow and becomes a real bound state.

Another treatment of impurity states which is more closely adapted to our present problem has been given by Slater and Koster.[13–15] They use a method based upon a Wannier function representation and a Green's

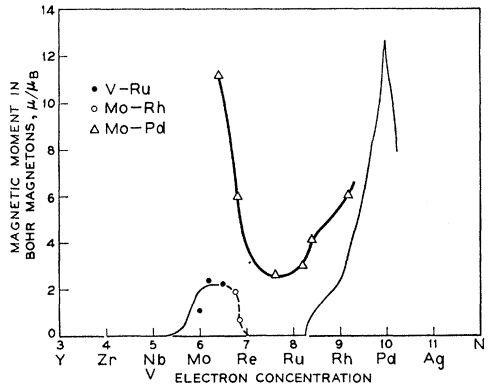

FIG. 5. Magnetic moment in Bohr magnetons of an ion atom dissolved in various second row transition metals and alloys as a function of electron concentration.

[12] J. Friedel, Supp. Nuovo cimento **7**, 287 (1958).
[13] G. F. Koster and J. C. Slater, Phys. Rev. **95**, 1167 (1954).
[14] G. F. Koster, Phys. Rev. **95**, 1436 (1954).
[15] G. F. Koster and J. C. Slater, Phys. Rev. **96**, 1208 (1954).

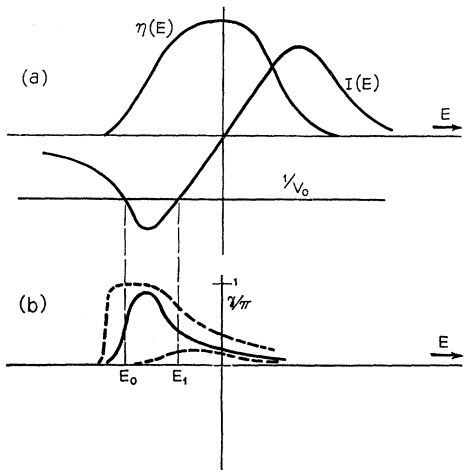

FIG. 6. (a) Typical curves of the function $\eta(E)$ and $I(E)$ as a function of energy; (b) the phase shift $\gamma(E)$ as a function of E for various values of V_0.

function solution that takes account of the band structure of the host metal. Although the method is perfectly general, the most useful results can be obtained by making the restrictive assumptions that only one band is involved with the impurity, and that the impurity potential is large only at the impurity site $r_0=0$. In this case, Slater and Koster find that the perturbed wave function is given by

$$\Psi_{\mathbf{k}}=\frac{1}{\sqrt{N}}\sum_i\left[e^{i\mathbf{k}\cdot\mathbf{r}_i}-\frac{V}{1+VG_E(0)}G_E(\mathbf{r}_i)\right]W(\mathbf{r}-\mathbf{r}_i), \quad (5)$$

where N is the number of lattice sites, $W(\mathbf{r}-\mathbf{r}_i)$ is the Wannier function associated with the ith site, V is the matrix component $(W(\mathbf{r}-\mathbf{r}_0)|V_{\mathrm{HF}}|W(\mathbf{r}-\mathbf{r}_0))$ of the self-consistent Hartree-Fock potential V_{HF}, and $G_E(\mathbf{r}_i)$ is the Green's function for the problem given by

$$G_E(\mathbf{r}_i)=\frac{1}{N}\sum_{\mathbf{k}}\frac{e^{i\mathbf{k}\cdot\mathbf{r}_i}}{E_{\mathbf{k}}-E}. \quad (6)$$

Although this was not done by Slater and Koster, their method can also be considered from the point of view of phase shifts.[16] We obtain thereby some particularly interesting results and insight into the nature of local states. From Eq. (6) we have

$$G_E(0)=\Omega\int\frac{\eta(E_{\mathbf{k}})dE_{\mathbf{k}}}{E_{\mathbf{k}}-E}, \quad (7)$$

where Ω is the atomic volume and $\eta(E)$ is the density of states per unit volume. If we define the principal part of this integral to be $-I(E)$, we have

$$G_E(0)=-I(E)+i\pi\Omega\eta(E). \quad (8)$$

With the additional assumption that the bands are spherical, it may be easily shown[16] from Eq. (5) that only the $l=0$ component of the scattered wave has a phase shift, and is given by

$$\gamma(E)=\tan^{-1}\left(\frac{\pi\Omega\eta(E)}{I(E)-1/V}\right). \quad (9)$$

The quantity $I(E)$ which enters this relation has been calculated for a special model by Slater and Koster.[15] An appreciation of the general shape of $I(E)$ can also be obtained by assuming a simple form for $\eta(E)$. Guided by such models, we have made a sketch in Fig. 6 of how $\eta(E)$ and $I(E)$ might appear in a typical case. As a rough rule of thumb, the peak values of I are about equal to the reciprocal of the width of the band. Let us suppose that V is negative (an attractive potential) and is large enough so that $1/V$ cuts $I(E)$ in two points as illustrated in Fig. 6(a). Then $\gamma(E)$ will have the shape shown by the solid line in Fig. 6(b). At the extreme left γ rises until it equals $\pi/2$ at the first intersection E_0, approaches π, falls to the value $\pi/2$ again at the second intersection E_1, and then approaches zero as E continues to increase. A curve very similar to this is given by Friedel in reference 12, Fig. 17. We may interpret the behavior of γ as follows. Just to the right of E_0, γ reaches nearly the value π, which we have seen means that approximately one whole state has been brought below this energy by the perturbation. In other words, a virtual state has been created in the vicinity of E_0 where $d\gamma/dE$ is large. Since γ falls to zero at the upper edge of the band, the total number of states is conserved, and it is clear that the virtual state has been removed from the vicinity of E_1.

The width of the virtual state is clearly controlled by the value of $\eta(E)$ at the point of intersection. If $\eta(E)$ is small the state will be very narrow. If V is increased from the value shown in Fig. 6(a) the intersection E_0 will move to the left so that $\gamma(E)$ will be given by the uppermost of the dotted curves in Fig. 6(b) and the state will become sharper. If the intersection is below the edge of the band, $\eta(E)$ will be zero and the state infinitely sharp. On the other hand as V becomes smaller, the virtual state will move up in the band and broaden. In fact, even if $1/V$ does not intersect $I(E)$, $\gamma(E)$ will still exist as shown in the lower dotted curve in Fig. 6(b) and there will be an accumulation of states in a broaden energy range.

We may also use Fig. 6(b) to visualize how the matrix element V can be made self-consistent. With a charge perturbation Ze in the lattice at r_0, we see from Eq. (4) that γ/π must equal $Z/2$ at the Fermi energy. With the Fermi energy determined by the bulk of the crystal remote from the perturbation, V must increase until $\gamma(E_f)$ has the proper value. With Z small enough, self-consistency can be obtained for E_f anywhere in the band. For larger values of Z, however, this model is restricted in its ability to achieve a self-consistent

[16] A. M. Clogston, Phys. Rev. **125**, 439 (1961).

value of V. Since we have limited ourselves to one band and a perturbation localized to one site, we can never displace more than one state below E_f. Beyond the point at which $I(E)=0$, γ/π cannot be larger than $\frac{1}{2}$, and if the band is full, γ can never be anything but zero. These restrictions mean physically that the model cannot supply enough charge to shield a very large perturbation, and that the self-consistent potential would be important at sites removed from r_0, or would cause appreciable distortion of nearby bands.

We have noted above that a virtual state is formed at the energy where $I(E)=1/V$. By reference to Eq. (5) we note that the square of the amplitude of the central Wannier function for the state of energy E is $(1/V)/\{[1/V-I(E)]^2+[\pi\Omega\eta(E)]^2\}$. The condition for the virtual state is therefore just the condition that the amplitude of the state be large at the impurity site.

B. Magnetization of Local States

We shall turn now to a discussion of the conditions under which a local state will magnetize. This problem has been treated recently in detail by Anderson[8] and Wolff.[9] The short discussion we give here is closely related to that presented by Wolff, although it differs in some details, and is based upon the Slater-Koster model introduced above.

The self-consistent Hartree-Fock potential for the impurity problem, operating on the Wannier function $W_\sigma(\mathbf{r}-\mathbf{r}_i)$, is given in the usual way by

$$\begin{aligned}
&V_{\mathrm{HF}}W_\sigma(\mathbf{r}-\mathbf{r}_i)\\
&=-\frac{Ze^2}{r}W_\sigma(\mathbf{r}-\mathbf{r}_i)+\sum_{\mathbf{k}'\sigma'}\left\{\left[\int\Psi_{\mathbf{k}'\sigma'}{}^*(\mathbf{r}')\frac{e^2}{|\mathbf{r}-\mathbf{r}'|}\right.\right.\\
&\left.\times\Psi_{\mathbf{k}'\sigma'}(\mathbf{r}')dV'\right]W_\sigma(\mathbf{r}-\mathbf{r}_i)\\
&-\left[\int\Psi_{\mathbf{k}'\sigma'}{}^{0*}(\mathbf{r}')\frac{e^2}{|\mathbf{r}-\mathbf{r}'|}\Psi_{\mathbf{k}'\sigma'}{}^0(\mathbf{r}')dV'\right]W_\sigma(\mathbf{r}-\mathbf{r}_i)\Big\}\\
&-\sum_{\mathbf{k}'}\left\{\left[\int\Psi_{\mathbf{k}'\sigma}{}^*(\mathbf{r}')\frac{e^2}{|\mathbf{r}-\mathbf{r}'|}W_\sigma(\mathbf{r}'-\mathbf{r}_i)dV'\right]\Psi_{\mathbf{k}'\sigma}\right.\\
&\left.-\left[\int\Psi_{\mathbf{k}'\sigma}{}^{0*}(\mathbf{r}')\frac{e^2}{|\mathbf{r}-\mathbf{r}'|}W_\sigma(\mathbf{r}'-\mathbf{r}_i)dV'\right]\Psi_{\mathbf{k}'\sigma}{}^0\right\},\quad(10)
\end{aligned}$$

where σ is the spin quantum number and the summation on k' is over filled states. We have added the direct potential due to the impurity nucleus, whereas the potential due to the unperturbed wave functions $\Psi_{\mathbf{k}}{}^0$ is not part of V_{HF} and has been subtracted. We can now use Eq. (10) to compute the matrix component V_σ which may be different for up and down spin electrons. We follow Wolff and approximate $\Psi_{\mathbf{k}\sigma}$ by using only that part depending on the central Wannier function. In that case we obtain for spin direction σ using Eq. (5),

$$V_\sigma=v+J\frac{1}{N}\sum_{E\sigma'}(1-\delta_{\sigma\sigma'})\left[\frac{1}{|1+V_{\sigma'}G_E(0)|^2}-1\right],\quad(11)$$

where

$$v=(W(\mathbf{r}-\mathbf{r}_0)\left|-\frac{Ze^2}{r}\right|W(\mathbf{r}-\mathbf{r}_0)),\quad(12)$$

and

$$\begin{aligned}
J=\Big(&W(\mathbf{r}-\mathbf{r}_0)W(\mathbf{r}'-\mathbf{r}_0)\left|\frac{e^2}{|\mathbf{r}-\mathbf{r}'|}\right|\\
&\times W(\mathbf{r}-\mathbf{r}_0)W(\mathbf{r}'-\mathbf{r}_0)\Big).\quad(13)
\end{aligned}$$

The quantity J appearing in Eq. (11) is the exchange self-energy of an electron in the central Wannier function and was first recognized by Anderson[8] as being important in determining whether or not a local state will magnetize. Being an exchange self-energy, it is much larger than ordinary exchange integrals and may become as large as 10 electron volts.[8]

Let us chose σ to be in the positive z direction. Then Eq. (11) may be written using Eq. (8)

$$V_\uparrow=-C+\frac{J\Omega}{V_\downarrow{}^2}\int_{-\infty}^{E_f}\frac{\eta(E)dE}{(1/V_\downarrow-I)^2+(\pi\Omega\eta)^2}.\quad(14)$$

The value of the constant C will be discussed below. Let us suppose now that $V_\downarrow$ is such that $1/V_\downarrow=I(E)$ at some energy $E_\downarrow$, and that the Fermi energy E_f is low

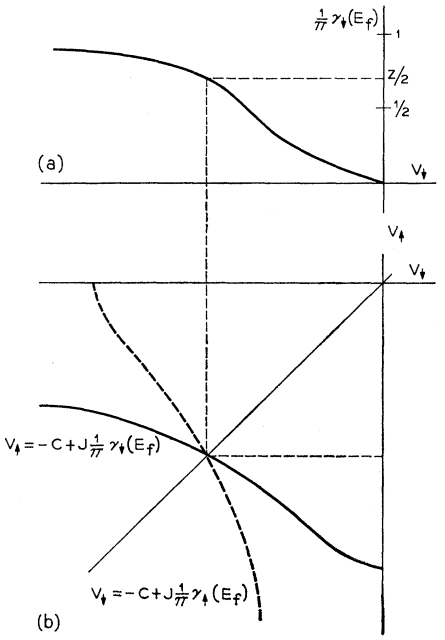

FIG. 7. (a) The phase shift at the Fermi level for down spin electrons as a function of $V_\downarrow$; (b) a curve of $V_\uparrow$ as a function of $V_\downarrow$ in a typical case resulting in one self-consistent solution.

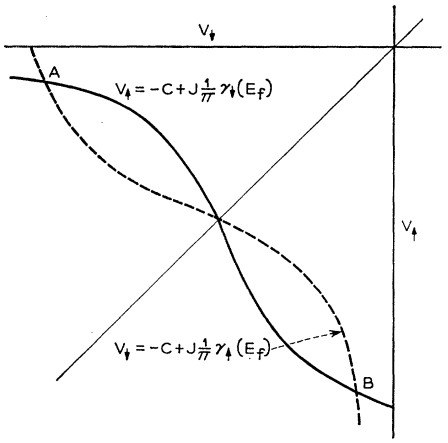

FIG. 8. A curve of $V_\uparrow$ as a function of $V_\downarrow$ in a case resulting in two self-consistent, magnetic solutions.

enough so that the range of integration does not include the second intersection shown in Fig. 6. The integrand in Eq. (14) will be large at $E=E_\downarrow$. In accordance with Eq. (9), we define a phase shift for electrons of spin direction σ by

$$\gamma_\sigma(E)=\tan^{-1}\left(\frac{\pi\Omega\eta(E)}{I(E)-1/V_\sigma}\right). \tag{15}$$

Upon differentiation, Eq. (15) becomes

$$\frac{d\gamma_\sigma}{dE}=-\frac{\pi\Omega\eta}{(1/V_\downarrow-I)^2+(\pi\Omega\eta)^2}\left[\left(\frac{1}{V_\downarrow}-I\right)\frac{1}{\eta}\frac{d\eta}{dE}+\frac{dI}{dE}\right]. \tag{16}$$

The result may be used to approximate the integrand in Eq. (14) in the vicinity of $E=E_\downarrow$, which then becomes

$$\begin{aligned}V_\uparrow&=-C-\frac{J}{V_\downarrow^2(dI/dE)_{E\downarrow}}\int_{-\infty}^{E_f}\frac{1}{\pi}\frac{d\gamma_\downarrow}{dE}dE \qquad (17)\\ &=-C-\frac{J}{V_\downarrow^2(dI/dE)_{E\downarrow}}\frac{1}{\pi}\gamma_\downarrow(E_f).\end{aligned}$$

Actually, it is clear from Eq. (6) that for energies low in the band $I(E)\simeq I/E$, measuring E from the center of the band so that $V_\downarrow^2(dI/dE)_{E\downarrow}\simeq -1$. Making this approximation in Eq. (17), we have finally

$$V_\uparrow=-C+J\frac{1}{\pi}\gamma_\downarrow(E_f). \tag{18}$$

Also, interchanging the roles of up and down spin we have

$$V_\downarrow=-C+J\frac{1}{\pi}\gamma_\uparrow(E_f). \tag{19}$$

Equations (18) and (19) can in principle be solved simultaneously for $V_\uparrow$ and $V_\downarrow$. The nature of the solution can best be understood graphically as shown in Figs. 7 and 8. In Fig. 7(a) we sketch the behavior of $(1/\pi)\gamma_\downarrow(E_f)$ as a function of $V_\downarrow$ determined from Eq. (15). If this curve is multiplied by J and displaced downward by an amount C, we obtain the solid curve in Fig. 7(b) representing Eq. (18). An interchange of up and down spins gives the dashed curve representing Eq. (19). Under the assumed conditions, the two curves intersect at a single point where $V_\uparrow=V_\downarrow=V$, so that in this case up and down spin electrons move in the same potential and the virtual state is unpolarized.

The common potential V determined in Fig. 7(b) also fixes the phase $\gamma(E_f)$. If the calculation could be carried out accurately without making the various simplifying assumptions that lead to Eq. (18), this value of $\gamma(E_f)$ would necessarily equal $(\pi/2)Z$ in order to satisfy the requirements of charge neutrality. The accurate curves then would be slightly different in shape from the approximate curves drawn in Fig. 7(b) but would intersect at the same value of V.

Let us consider next a case where J is considerably larger. Equations (18) and (19) would then lead to the curves shown in Fig. 8, which now exhibit three intersections. It is easy to see that the intersection for $V_\uparrow=V_\downarrow$ is unstable in this case since a small increase in $|V_\downarrow|$ leads to a decrease in $|V_\uparrow|$, which then corresponds to a larger increase in $|V_\downarrow|$. Conversely, the intersections at A and B are stable. These roots correspond to unequal values of $V_\uparrow$ and $V_\downarrow$, and therefore to a different accumulation of up and down spin electrons. The virtual state consequently is magnetized, and the two intersections correspond to opposite senses of polarization.

The condition for there to be two roots to Eqs. (18) and (19) is clearly that $|dV_\uparrow/dV_\downarrow|$ be greater than unity at the symmetric intersection where $V_\uparrow=V_\downarrow=V$. Differentiating Eq. (18) we find

$$\frac{dV_\uparrow}{dV_\downarrow}=-J\frac{\Omega\eta(E_f)}{[I(E_f)-1/V]^2+[\pi\Omega\eta(E_f)]^2}\frac{1}{V^2}. \tag{20}$$

Suppose that the virtual level corresponding to potential V is at $E=E_0$. We define the width Δ of the virtual level by the relation $(1/\pi)(d\gamma/dE)_{E_0}\Delta=1$. Then from Eq. (16) we have,

$$\Delta=-\pi^2\Omega\eta(E_0)\Big/\left(\frac{dI}{dE}\right)_{E_0}. \tag{21}$$

We now approximate by letting

$$I(E_f)=I(E_0)+(dI/dE)_{E_0}(E_f-E_0),$$
$$\eta(E_f)=\eta(E_0) \quad \text{and} \quad I(E)=1/E.$$

Then Eq. (20) becomes

$$\frac{dV_\uparrow}{dV_\downarrow}=-J\frac{\Delta}{\pi^2(E_f-E_0)^2+\Delta^2}, \tag{22}$$

which is the result found by Anderson[8] and Wolff.[9]

Equation (22) is an important relation. If the virtual state is at the Fermi level ($E_f=E_0$), it shows that J must be greater than the width Δ if the state is to polarize. This is what makes so important Anderson's observation that J is much larger than an ordinary exchange integral. Furthermore, the further the virtual state is below the Fermi level the harder it is to magnetize. Also, we note that as E_0 increases in energy from the bottom of the band Δ becomes greater, approaching infinity at the point where $dI/dE=0$. We will use these results in the next section in discussing the occurence of local moments.

We shall conclude this section by discussing the situation when the Fermi level is so high in the band that it lies above the second intersection E_1 shown in Fig. 6. In this case, we find that we must replace Eq. (18) approximately by the expression

$$V_\uparrow=-C+J\left[1-\frac{1}{V_\downarrow^2(dI/dE)_{E_1}}[\gamma(E_f)-1]\right]. \quad (23)$$

We can make a sketch of this relation, and the relation obtained by interchanging up and down spins, as we did before, with the result shown in Fig. 9. Because of the change in sign of dI/dE, every intersection of the two curves now corresponds to $V_\uparrow=V_\downarrow$, and the virtual state therefore cannot magnetize. The intersection is stable and must correspond to the value of V required for charge neutrality.

C. Occurrence of Localized Moments

Let us now consider how the ideas we have introduced above about localized wave functions, and the conditions under which they are likely to magnetize, can be used to explain the occurrence of localized moments in dilute alloys of Fe in the 4d metals. We should first of all examine what is known about the band structure of the transition metals. The most reliable and complete band calculations made to date have been done for body centered cubic iron by Stern[17] and Wood.[18]

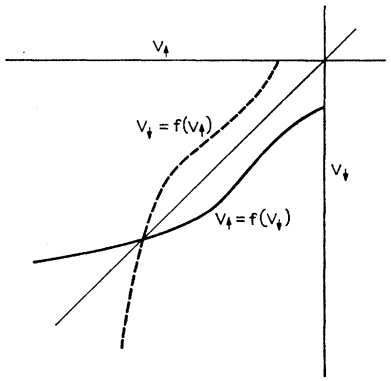

FIG. 9. A curve of $V_\uparrow$ as a function of $V_\downarrow$ in a case which leads only to nonmagnetic solutions.

[17] F. Stern, Phys. Rev. **116**, 1399 (1959).
[18] J. H. Wood (to be published).

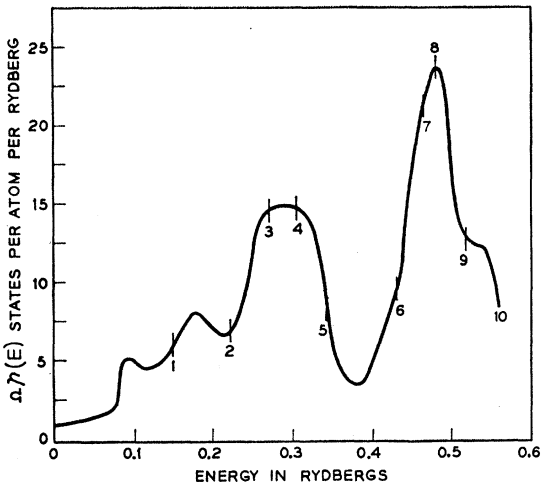

FIG. 10. The density of states per atom per rydberg as a function of energy for body centered iron according to J. H. Wood.

In the absence of band calculations for the second row transition metals, we shall assume that the iron calculations have some validity for the body centered cubic 4d metals. The iron calculations are made for a nonmagnetic state and do not attempt to account for the ferromagnetism of iron. This restriction is, however, an appropriate one for the 4d case.

Wood has used his band calculation to determine a density of states for iron,[18] and his curve is reproduced in Fig. 10. It is characterized by the double-humped structure usually assumed for the d band metals. The integrated number of electrons N per atom below various energies is marked on the curve. In the discussion that follows, we shall assume that the rigid band model applies sufficiently well for our purposes so that we can treat the density of states curve as being fixed while the electron concentration varies from 5 to 7 per atom proceeding from Nb to Re. The accuracy of this assumption is, of course, dubious and may account for the differences between Fig. 10 and the results of low temperature specific heat measurements by Cheng, Wei and Beck.[19] These authors find a minimum in specific heat between $N=5$ and 6 in agreement with Fig. 10 but find a peak in specific heat between $N=6$ and 7 rather than at $N=8$.

For the bcc structure, the points Γ and H in the Brillouin zone have full cubic symmetry while the point P has tetrahedral symmetry.[20] The doubly degenerate levels e_g, and triply degenerate levels t_{2g} are not split at these points. Moreover the order of levels at P is the same as at Γ. As a consequence, it is clear from a consideration of the energy bands calculated by Stern[17] that the large peak in density of states at $N=8$ largely derives from atomic states of symmetry e_g,

[19] C. H. Cheng, C. T. Wei, and P. A. Beck, Phys. Rev. **120**, 426 (1960).
[20] L. P. Bouckaert, R. Smoluchowski, and E. Wigner, Phys. Rev. **50**, 58 (1936).

although there will be some contribution from other bands. It will be noted that the area under the peak corresponds to just about four electrons. This fact has a direct relation to our experiments and accounts for the fact that the alloys just beyond Mo develop a maximum of 2 Bohr magnetons per atom.

N=5 to 7

Within the frame work of the rigid band model then, let us consider the course of events proceeding from $N=5$ to 7 for the alloys shown in Fig. 1. Except for the last member of the series, Re, these alloys all have the bcc structure. We start at $N=6$. At this point, the iron nucleus plus core electrons constitutes an impurity with two excess positive charges. We suppose that half the shielding charge is to be provided by each of the e_g derived bands. Each band must therefore form a virtual state just at the Fermi level. We have seen in the last section that this is the optimum condition for magnetization of the state, and that the necessary condition is $J>\Delta$. From Fig. 11 we see that E_0 is about 0.05 ry so that $1/(dI/dE)_{E_0}\simeq -E_0^2=25\times10^{-4}$; also $\Omega\eta(E_0)$ for each band is about 5 states per ry. Using Eq. (21) we obtain $\Delta\simeq 0.1$ ry or 1.4 electron volts. We have estimated earlier that J may be as large as 10 electron volts, so that we should definitely expect the virtual states to magnetize at this point, giving a net moment of approximately 2 Bohr magnetons per iron atom as observed.

Suppose now that we increase the electron concentration toward $N=7$. Two things happen. First, since the iron core now becomes an impurity with less than two excess charges, the virtual states must move to a higher energy than the Fermi level. Secondly, the width of the virtual states will increase rapidly. Both these events are unfavorable to polarization, and we have seen in Fig. 1 that at $N=7$ the states have already demagnetized.

On the other hand, suppose that the electron concentration decreases from $N=6$ to $N=5$. It is evident that the burden of shielding the three excess nuclear charges will now be assumed partly by the lower half of the band, and that the virtual levels derived from the upper half of the band will tend again to lie at an energy higher than the Fermi level and be more difficult to magnetize. Since the Fermi level is above the lower half of the band, we cannot expect any polarization from this source. The theory as presently developed cannot hope to deal with this complex interplay between the various bands, but we see experimentally that at $N=5$ the shielding of the 3 nuclear charges is being effected by states that are too diffuse to magnetize. We have attempted in Fig. 11 to visualize the three conditions described above that lead to the appearance of a localized moment between $N=5$ and 7.

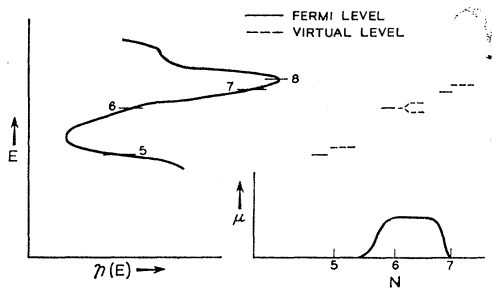

FIG. 11. A schematic description of the process leading to the appearance of a local magnetic moment between $N=5.5$ and $N=7$.

N=8 to 9

As may be observed in Fig. 1, the local moment, after disappearing at $N=7$, reappears between $N=8$ and 9 and approaches a value of about $2\mu_B$ again at $N=9$. On the basis of our previous discussions, we may give the following interpretation to these events. As N increases beyond 8, the Fermi level has certainly risen above the major part of the 4*d* band and the general trend of the density of states must be to decrease. This is illustrated for example in Fig. 10. Although Fig. 10 applies to the bcc structure the trend should also be true for the present case even though the structure is no longer bcc but starts as hcp at ruthenium and ends as fcc at rhodium.

As the electron concentration increases beyond $N=8$, the iron nucleus plus core electrons will begin to act like a negative impurity in the lattice. We may expect, therefore, with increasing N that a virtual state will form at an energy somewhat smaller than the Fermi energy. In a mirror image of the previous process, this virtual level will tend to overtake the Fermi energy as N increases and will eventually magnetize, as happens experimentally beyond $N=8.25$.

D. Giant Moments; $N=9$ to 10

An outstanding feature of Fig. 1 is the occurence of very large moments beyond an electron concentration of $N=9$. Crangle,[6] Gerstenberg[5] and Bozorth *et al.*[7] have observed these large moments in the ferromagnetic state for dilute alloys of Fe and Co. The present measurements show that these giant moments increase systematically with increasing Pd content in the dilute iron alloys beyond Rh, and that the large moment is also characteristic of the paramagnetic state of these alloys. As made evident by the clear correspondence between Fig. 1 and Fig. 3, the occurence of giant moments is closely related to the high susceptibilities encountered in the Rh—Pd system for compositions near Pd. This correspondence extends to the location of the peak value of moment and susceptibility respectively at a composition near 5 at. % rhodium.

The occurence of a peak in susceptibility near Pd can be interpreted on the basis of the rigid band model as a peak in density of states near the edge of the band. This is contrary to our assertion that the general trend

of the density of states in this region of the periodic table must be to decrease. Actually, however, only a small number of states per atom, about 0.1, are included in this peak. We can easily calculate from the specific heat data of Budworth, Hoare, and Preston[11] that the maximum in density of states at 5 at. % rhodium corresponds to about 2 states per electron volt. The width of the peak, therefore, in energy is very narrow, about 0.05 electron volt. Superimposed on a state density curve like Fig. 10, the peak would be extremely high and narrow. Evidently there are not enough states in this peak to cause the virtual state to demagnetize.

We can give a reasonable explanation of the occurence of giant moments in the dilute iron Rh—Pd alloys and their relation to the susceptibility of the matrix by making further use of the ideas introduced in previous sections. Let us take the Hartree-Fock potential given by Eq. (10) and evaluate its matrix components between Wannier functions located at sites which are nearest neighbors to the impurity atom. Then we find approximately,

$$(W_\uparrow(\mathbf{r}-\mathbf{r}_\alpha)|V_{\mathrm{HF}}|W_\uparrow(\mathbf{r}-\mathbf{r}_\alpha)) -(W_\downarrow(\mathbf{r}-\mathbf{r}_\alpha)|V_{\mathrm{HF}}|W_\downarrow(\mathbf{r}-\mathbf{r}_\alpha))=-2S_0J', \quad (24)$$

where α indicates a nearest neighbor site to an impurity atom, and S_0 and J' are given by

$$2S_0=\frac{1}{N}\sum_E\left[\frac{1}{|1+V_\uparrow G_E(0)|^2}-\frac{1}{|1+V_\downarrow G_E(0)|^2}\right], \quad (25)$$

$$J'=\left(W(\mathbf{r}-\mathbf{r}_\alpha)W(\mathbf{r}'-\mathbf{r}_0)\left|\frac{e^2}{|\mathbf{r}-\mathbf{r}'|}\right| \times W(\mathbf{r}-\mathbf{r}_0)W(\mathbf{r}'-\mathbf{r}_\alpha)\right). \quad (26)$$

S_0 is the total spin associated with the central Wannier function, and J' is the ordinary exchange integral between the central Wannier function and the nearest neighbor Wannier functions. We thus effectively introduce at each near neighbor site a spin-dependent impurity potential $V_{\alpha\sigma}$ given by

$$V_{\alpha\uparrow}=-S_0J', \quad V_{\alpha\downarrow}=S_0J'. \quad (27)$$

Each neighbor therefore will be a center for the accumulation of up and down spin electrons. Because $V_{\alpha\uparrow}$ and $V_{\alpha\downarrow}$ are different, there will be a net accumulation of spin at each neighbor in accordance with Eq. (15) given by

$$2S_\alpha=\frac{1}{\pi}\tan^{-1}\left(\frac{\pi\Omega\eta(E_f)}{I(E_f)-1/V_{\alpha\uparrow}}\right) -\frac{1}{\pi}\tan^{-1}\left(\frac{\pi\Omega\eta(E_f)}{I(E_f)-1/V_{\alpha\downarrow}}\right). \quad (28)$$

Under any expected circumstances $V_{\alpha\uparrow}$ and $V_{\alpha\downarrow}$ will be much smaller than $I(E_f)$, so that Eq. (28) becomes

$$S_\alpha=\frac{1}{\pi}\tan^{-1}[\pi\Omega\eta(E_f)S_0J']. \quad (29)$$

The calculation leading to Eq. (29) is not quite correct because of effects connected with the interference of wave functions scattered from each of the Z nearest neighbors of the impurity site. Slater and Koster[15] have shown how to handle correctly a perturbation extending over several near neighbors, but the interference effects are rather small and will be neglected here. Consequently, we shall write for the total spin S_T associated with the localized spin S_0

$$S_T=S_0+\frac{Z}{\pi}\tan^{-1}[\pi\Omega\eta(E_f)S_0J']. \quad (30)$$

If the argument of the arc tangent is small, Eq. (30) becomes approximately

$$S_T\simeq S_0+Z\Omega\eta(E_f)S_0J'. \quad (31)$$

This is exactly the result that would be obtained for the average polarization using the perturbation theory method of Ruderman and Kittel[21] and Yosida.[22] In arriving at Eq. (30) we have supposed that the polarization of the matrix by the local spin will involve only the states of one band. That is, we are assuming for simplicity that the high susceptibility of the Rh—Pd alloys of high Pd concentration arises from only one band.

Bozorth *et al.*[10] have proposed a model to explain the giant moments observed in Pd—Co alloys. They suppose that an exchange interaction between the impurity spin and the nearest neighbor Pd atom polarizes each such atom to the extent of the 0.6 hole per atom presumed to exist in the Pd 4*d* band. Although this model leads to approximately the observed moment for $Pd_{0.99}Fe_{0.01}$, it cannot easily be reconciled with the moments observed in the Pd—Rh dilute iron alloys.

The theory we propose here makes no reference to the number of unfilled states in the 4*d* band, but depends instead upon the density of states at the Fermi surface. According to Eq. (30), S_T will increase with increasing susceptibility since $\eta(E_f)$ will increase. We may therefore account in a qualitative fashion for the observed correspondence between local moment and susceptibility. Since we have no experimental determination of S_0, but only of S_T, we cannot easily test the functional form of Eq. (30). We may, however, see if reasonable assumptions about the parameters S_0 and J' can account for the experimental moments.

The quantity $\Omega\eta(E_f)$ appearing in Eq. (30) can be

[21] M. A. Ruderman and C. Kittel, Phys. Rev. **96**, 99 (1954).
[22] K. Yosida, Phys. Rev. **106**, 893 (1957).

related to the molar susceptibility by the expression

$$\Omega\eta(E_f)=\frac{M_0}{2\mu_B{}^2}\chi_M$$

$$=1.55\times10^4\,\chi_M \text{ states per electron volt.} \quad (32)$$

For Pd at 100°K, χ_M is about 800×10^{-6}. Hence $\Omega\eta(E_f)$ is 12.4 states per electron volt. Actually χ_M in Pd may be enhanced by exchange, but we can easily show in that case that we should use in Eq. (30) an effective value of $\Omega\eta(E_f)$ related to the observed susceptibility by Eq. (32). An order of magnitude guess for a reasonable value of J' is 0.1 electron volt, so that $\Omega\eta(E_f)J'$ is about 1.2. From the shape of the curve of μ/μ_B versus N in Fig. 1, we may estimate that S_0 is about 1 corresponding to a moment of 2 Bohr magnetons. From Eq. (30), we find $S_T=6$ so that the total expected moment is 12 Bohr magnetons.This close agreement with the observed value is, of course largely accidental since we have made a very crude estimate of J'. Actually, however, Eq. (30) is rather insensitive to the value of J' for large values of the argument of the arc tangent. If we chose a value of J' equal to 0.05 electron volt, the predicted value of S_T would drop only to 10 μ_B, while for J' infinite it can get no larger than 14 μ_B. The model appears therefore to give an adequate account of the giant moments found near palladium in terms of the unusually high susceptibility of the matrix.

V. CONCLUSION

In the preceding sections we have presented experimental data that show the systematic occurence of localized magnetic moments when iron is present in small amounts in alloys of the second row transition metal elements. These moments first appear at an electron concentration of 5.5, disappear at $N=7$, reappear at $N=8.25$ and continue to the end of the period. Within the confines of the present development of the theory of localized states and of the band tructure of the transition metals, we have been able to account for these general features of the experiments.

A second notable result of the measurements we report is the occurence of very large moments in the dilute iron alloys of rhodium and palladium. In order to obtain meaningful results from the paramagnetic susceptibility data, we have been forced to take account of the temperature variation of the polarization of the matrix by the local moment. We find in fact that the total local moment in various alloys is strongly correlated with the susceptibility of the matrix. These giant moments have been observed before in measurements of the saturation magnetization of the ferromagnetic alloys of iron and cobalt with palladium, but we see now that they are also characteristic of the paramagnetic state and of a range of alloys near palladium. We have introduced a theory that describes the polarization of the matrix by a local moment and which accounts for the very large moment of approximately 11 Bohr magnetons seen in palladium. An interesting feature of this calculation is that the result is outside the range of perturbation theory.

There are various directions in which a useful extension could be made of the results reported here. A similar study could be made of dilute alloys of manganese, cobalt, and nickel, and the work could be extended to alloys of the 5*d* group. The method appears to offer a powerful approach to the problem of understanding the nature of ferromagnetism in the transition metals.

ACKNOWLEDGMENTS

We would like to recognize many helpful and stimulating conversations with our colleagues during the course of this work, in particular with P. A. Wolff, P. W. Anderson and T. Moriya. We also wish to thank Mrs. Vera Compton for x-ray studies and Miss S. M. Vincent for x-ray fluorescence analysis of the large number of alloys it was necessary to prepare.